A NUMERICAL STUDY USING HYBRID NANOFLUID TO CONTROL HEAT AND MASS TRANSFER IN A POROUS MEDIA: APPLICATION TO DRYING OF BUILDING BRICKS

Mohamed Bechir BEN HAMIDA[*1,2,3]

[1]College of Engineering, Imam Mohammad Ibn Saud Islamic University (IMSIU), Riyadh, Saudi Arabia

[2]Research Laboratory of Ionized Backgrounds and Reagents Studies (EMIR), Preparatory Institute for Engineering Studies of Monastir (IPEIM), University of Monastir, Monastir City, Tunisia

[3]Higher School of Sciences and Technology of Hammam Sousse (ESSTHS), University of Sousse, Tunisia

[*] Corresponding author; E-mail: benhamida_mbechir@yahoo.fr

This paper's main objective is to perform a numerical analysis of the heat and mass transfer that occurs during the mixed convective drying of porous walls containing hybrid nanofluid. The porous wall, used to dry the brick, is positioned in a vertical channel and has three different phases: a solid phase, a hybrid nanofluid phase, and a gas phase. In order to accomplish this, we created a two-dimensional code using Comsol Multiphysics to resolve the equations relating mass, momentum, species, and energy. The impact of various parameters, including ambient temperature, initial hybrid nanofluid saturation, and nanoparticle volume percent, on heat and mass transmission was examined after this numerical code's validity. As the volume percentage of nanoparticles rises, it is discovered that the temperature of the porous medium is significantly lowered. The heat and mass transfer of the Water-Alumina-MgO hybrid nanofluid has been discovered to be much less than that of pure water and the Water-Al$_2$O$_3$-SiO$_2$. As the ambient temperature rises, it takes less time for the second phase to dry.

Key words*: Drying, Porous media, Hybrid nanofluids, Mixed convection, Heat and mass transfer, Comsol Multiphysics.*

1. Introduction

Owing to its vast applicability in engineering sectors such as solar collectors, heat exchangers, oil recovery, geothermal energy, building construction, and in particular drying processes [1-2], heat transfer and fluid flow and in porous media have recently been the subject of numerous investigations. [3-6].

As a result, the high energy consumption of porous solids during drying has piqued scientific and technological interest in a wide range of commercial applications, including ceramics, food, wood [7], paper, building materials [8], textile, steel Balls [9], and brick that is the focus of this research.

Nanofluids have become a popular research topic in recent years due to their superior thermal properties. A nanofluid is a fluid that contains nanometer-sized particles (less than 100 nm in diameter) or fibers suspended in a base fluid including water [10-15], ethylene glycol [16-17], or oil [18].

The porous media is enhanced by using nanofluid. Sheikholeslami [19] investigated a model for an energy storage system including the mixture of paraffin and ZnO nano-powders considering porous media. The nanofluid is used for cooling heat sink and other device [20-23]. Massoudi and Ben Hamida [24] improve the MHD radiative CNT-50% of water and ethylene glycol nanoliquid performance in cooling an electronic heat sink featuring wavy fins. Recently, the incorporation of nanofluid is used by Sheikholeslami and Jafaryar [25] in the Thermal assessment of solar concentrated system with utilizing CNT nanoparticles and complicated helical turbulator. In addition, Sheikholeslami and Ebrahimpour [26] improve the of linear Fresnel solar system utilizing Al_2O_3-water nanofluid and multi-way twisted tape.

Nowadays, it was found that hybrid nanofluid which contains base fluid and 2 kinds of nanoparticles is much better than nanofluid and uses to improve heat transfer in several areas.

The performance of bubble absorbers can be improved in order to decrease their size by using hybrid nanofluid (Alumina-Copper) as a cooled NH_3/H_2O absorption system [27]. Ben Jaballah et al [28] were also revealed that as the solid volume percentage increases, both the heat load on the absorber and the mass absorption flux rise. In addition, it was discovered that there is an ideal absorber length needed for full absorption when employing hybrid nanofluid as a cooling medium. The best candidate for improving the performance of NH_3/H_2O absorption is advised to use hybrid nanofluid to remove heat from the absorber.

In order to cool the Light emitting Diode, Ben Hamida and Hatami [29] used four different hybrid nanofluids with water as the base fluid (TiO_2-Al_2O_3, TiO_2-CuO, Al_2O_3-Cu and Al_2O_3-CuO). The junction temperature of the LED is reduced by all types of hybrid nanofluid, according to the results. Al_2O_3-TiO_2 got the highest Nusselt number. Additionally, the local and average Nusselt numbers were enhanced by 5.19% and 0.43%, respectively, by increasing the concentration of nanoparticles by 0.01.

For the electroosmotic flow of a Fe_3O_4-Cu/H_2O hybrid nanofluid with peristaltic propulsion, Abbassi et al. [30] look at the thermodynamic analysis. A mixture of copper and iron oxide nanoparticles in water is called a hybrid nanofluid. According to the findings, adding nanoparticles to a hybrid nanoliquid lowers its temperature and entropy generation. When Joule heating and electroosmotic parameters are improved, heat transfer rate increases. Fluid velocity decreases as the Helmholtz-Smoluchowski velocity and Hartmann number rise. In comparison to base fluid and traditional mono nanofluid (Fe_3O_4-H_2O), hybrid nanofluid (Fe_3O_4-Cu/H_2O) has more noticeable thermal performance (H_2O).

The nanfluid hybrid was employed by Sheikholeslami [31] to address the issue of solar system equipped with innovative turbulator. Ben Hamida and Hatami [32] investigate the heated fins geometries on the heat transfer of a channel filled by hybrid nanofluids under the electric field.

In this present article, the hybrid nanofluid is used for in drying the brick as building application. For this, a numerical study was using Comsol Multiphysics of the mass and heat transfer during mixed convective drying of porous wall containing Water-Al_2O_3-MgO. Then, a comparison

with another nanohybrid Water-Al_2O_3-SiO_2, which is also generally widely used in building materials in order to choose the best.

2. Formulation of the problem

Figure 1 presents the configuration of the brick which is the subject of our study. It's having a length (L=300 mm) and thickness (e=12 mm). It is considered as an unsaturated porous vertical wall, made up of an inert and hard solid phase, a hybrid nanofluid phase (Water-Al_2O_3-MgO or Water-Al_2O_3-SiO_2), and a gas phase that contains both air and water vapor. The upper and lower faces of the porous vertical wall face, as well as the left vertical face, are adiabatic and impermeable. The permeable interface of the vertical channel of width (W=100 mm) is on the porous vertical wall's right-hand side. External downward laminar flow of a mixture of air and water vapor with adjustable inflow variables is applied to the porous vertical wall.
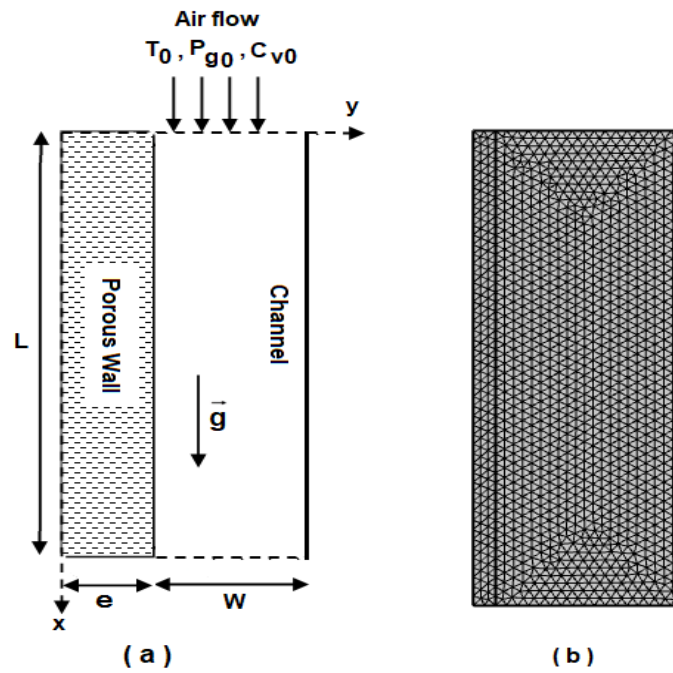

Fig. 1. (a)-Schematic of physical problem; (b) - Mesh used in Comsol Multiphysics

2.1. Hypotheses

The following hypotheses are taken into account in this study:

- Heat and mass are transmitted in both directions (x,y).
- The Soret and Dufour effects, as well as viscous dissipation and compression work, are not taken into account.
- Local thermal equilibrium presents between the solid, liquid, and gas phases.
- The concepts dispersion and tortuosity are translated to diffusion expressions.
- Radiative heat transmission is not taken into account.
- The approximations for the boundary layer are accurate.
- The porous media is isotropic and homogeneous.
- The channel-porous medium at the interface is semi-permeable.

- The hybrid nanofluid is treated as one liquid phase.
- The nanoparticles are uniformly dispersed.

2.2. Governing equations

In two-dimensional Cartesian coordinates (x, y), the controlling equations for the conservation of mass, momentum, energy, and species are:

2.2.1 Inside the channel

- *Mass conservation equation*

$$\frac{\partial(\rho_g U)}{\partial x} + \frac{\partial(\rho_g V)}{\partial y} = 0 \tag{1}$$

- *Momentum equation*

$$\rho_g U \frac{\partial U}{\partial x} + \rho_g V \frac{\partial U}{\partial y} = -\frac{\partial p_g}{\partial x} + \frac{\partial}{\partial y}\left(\mu_g \frac{\partial U}{\partial y}\right) - \gamma \rho_g \left[\beta(T - T_0) + \beta^*(C_V - C_{V0})\right] g \tag{2}$$

In this situation, the factor γ is equal to one for free or mixed convection and zero for forced convection.

- *Energy equation*

$$\rho_g C_{pg}\left(U \frac{\partial T}{\partial x} + V \frac{\partial T}{\partial y}\right) = \frac{\partial}{\partial y}\left(\lambda_g \frac{\partial T}{\partial y}\right) + \rho_g D_V (Cp_V - Cp_a)\frac{\partial T}{\partial y}\frac{\partial C_V}{\partial y} \tag{3}$$

- *Concentration equation*

$$\rho_g U \frac{\partial C_V}{\partial x} + \rho_g V \frac{\partial C_V}{\partial y} = \frac{\partial}{\partial y}\left(\rho_g D_V \frac{\partial C_V}{\partial y}\right) \tag{4}$$

2.2.2 Inside the porous media

o *Mass conservation equations*
- *Hybrid nanofluid phase*
The mass conservation equation for the hybrid nanofluid phase with a constant hybrid nanofluid density, as follows:

$$\frac{\partial \varepsilon_{hnf}}{\partial t} + \nabla \overline{V_{hnf}} = -\frac{m^*_V}{\rho_{hnf}} \tag{5}$$

- *Gas phase*
This phase's average density $\left(\overline{\rho_g}\right)^g$ varies; the following is the gas phase's mass conservation equation:

$$\frac{\partial \overline{\rho_g}}{\partial t} + \nabla\left(\overline{V_g} \times \left(\overline{\rho_g}\right)^g\right) = m^*_V \tag{6}$$

4

- *Vapor phase*

$$\frac{\partial \overline{\rho_V}}{\partial t} + \nabla\left(\overline{V_V} \times \left(\overline{\rho_V}\right)^V\right) = m^*v \tag{7}$$

o Darcy's law is used to determine the average velocities of the gas phase $\overline{V_g}$ and the hybrid nanofluid phase $\overline{V_{hnf}}$

- *Hybrid nanofluid phase*

$$\overline{V_{hnf}} = -\frac{K\,K_{hnf}}{\mu_{hnf}}\left[\nabla\left(\left(\overline{P_g}\right)^g - P_c\right) + g\,\rho_{hnf}\right] \tag{8}$$

- Gas phase

$$\overline{V_g} = -\frac{K\,K_g}{\mu_g}\nabla\left(\overline{P_g}\right)^g \tag{9}$$

o *Energy conservation equation*

$$\frac{\partial\left[\overline{\rho C_p T}\right]}{\partial t} + div\left[\left(\overline{\rho_{hnf}}\,Cp_{hnf}\,\overline{V_{hnf}} + \sum_{k=a,v}\left(\overline{\rho_k}\right)^g Cp_{pk}\,\overline{V_k}\right)\overline{T}\right]$$
$$= div\left[\lambda_{eff}\;grad\left(\overline{T}\right)\right] - m^*v\,\Delta H_{vap} \tag{10}$$

The formula used to compute ΔH_{vap}, or the latent heat of vaporization function of temperature, is:

$$\Delta H_{vap} = \Delta H^0_{vap} - \left(Cp_V - Cp_{hnf}\right)\overline{T}\right) \tag{11}$$

Where ΔH^0_{vap} is the latent heat of vaporization at the temperature of zero Kelvin.

2.2.3   Initial and boundary conditions

o Initial conditions
  - At the inlet of the channel, the fluid state variables (T_0, C_{v0}, U_0, and P_{g0}) are assumed as constant.

o Boundary conditions
o *For the channel's fluid*
  - The gas phase's longitudinal and transverse velocities are expressed as:

$$U(x,L) = 0 \quad and \quad V(x,L) = -\frac{D_V}{1-C_V}\frac{\partial C_V}{\partial y} \tag{12}$$

  - For the channel's right face:

$$U(x,L+e) = 0 \quad and \quad V(x,L+e) = 0 \tag{13}$$

- The following equation evaluates the local interfacial evaporating mass flux:

$$m^*v(x,L) = \rho_g\,V(x,L) \quad for \quad 0 \le C_V(x,L) < 1 \tag{14}$$

-The channel's right vertical plate is maintained isothermally and at ambient temperature.

o *For the porous media*

  - The heat and mass fluxes are equal to zero on the adiabatic and impermeable sides:

  For x = 0, x = L and $0 \leq y \leq l$:

$$\lambda_{eff} \frac{\partial \overline{T}}{\partial x} = 0 \; ; \left(\overline{V_V}\right)_x = 0 \; ; \left(\overline{V_g}\right)_x = 0 \;\; and \;\; \left(\overline{V_{hnf}}\right)_x = 0 \tag{15}$$

  For $0 \leq x \leq L$ and y = 0:

$$\lambda_{eff} \frac{\partial \overline{T}}{\partial y} = 0 \; ; \left(\overline{V_V}\right)_y = 0 \; ; \left(\overline{V_g}\right)_y = 0 \;\; and \;\; \left(\overline{V_{hnf}}\right)_y = 0 \tag{16}$$

  - On the permeable face (0 < x < L, y = l), heat and mass fluxes are given as follows:

$$\lambda_{eff} \frac{\partial \overline{T}}{\partial y} + \Delta H_{vap} \left(\overline{\rho_{hnf}} \, \overline{V_{hnf}}\right)_y = h_{tx}\left(T_0 - \overline{T}\right) \tag{16}$$

$$\overline{\rho_{hnf}} \, \overline{V_{hnf}} + \left(\overline{\rho_V}\right)^g \overline{V_V} = h_{mx}\left(\left(\overline{\rho_V}\right)^g - \rho_{V0}\right) \tag{17}$$

With h_{tx} and h_{mx} are coefficients of heat and mass transfer, respectively.

- As a function of temperature and hybrid nanofluid saturation, the equilibrium vapor pressure is determined:

$$P_V = P_{VS} \exp\left[-\frac{2\sigma M_V}{r\,RT\,\rho_{hnf}}\right] \tag{18}$$

With P_{vs} is the saturated vapor pressure at interface, given by [33]:

$$P_{VS} = 10^5 \exp\left[65.832 - 8.2\,Ln\,(T_{int}) + 0.005717\,T_{int} - \frac{7235.46}{T_{int}}\right] \tag{19}$$

2.2.4 *Proprieties of hybrid nanofluid thermophysical*

  All expressions of base fluid which water are function of temperature according to its range as follows:

Dynamic viscosity of water [34]**:**

273.15 K < T < 473.15 K :
$$\mu = 1.3799566804 - 0.021224019151*T + 1.3604562827*10^{-4}*T^2 - 4.6454090319*10^{-7}*T^3 + 8.9042735735*10^{-10}*T^4 - 9.0790692686*10^{-13}*T^5 + 3.8457331488*10^{-16}*T^6 \tag{20}$$

473.15 < T < 553.15 K :
$$\mu = 0.00401235783 - 2.10746715*10^{-5}*T + 3.85772275*10^{-8}*T^2 - 2.39730284*10^{-11}*T^3 \tag{21}$$
T in K and dynamic viscosity in Pa.s

Thermal Capacity of water [34]**:**

273.15 < T < 553.15 K

6

Cp = 12010.1471 - 80.4072879*T + 0.309866854*T^2 - 5.38186884*10^{-4}*T^3 + 3.62536437*10^{-7}*T^4 (22)

T in K and Thermal Capacity in J/(kg*K)

Mass density of water [34]:

273.15 < T < 293.15 K

$$\rho = 0.000063092789034*T^3 - 0.060367639882855*T^2 + 18.9229382407066*T - 950.704055329848$$ (23)

293.15 < T < 373.15 K

$$\rho = 0.000010335053319*T^3 - 0.013395065634452*T^2 + 4.969288832655160*T + 432.257114008512$$ (24)

T in K and mass density in kg/m^3

Thermal conductivity of water [34]:

273.15 < T < 1000 K

$$\lambda = -0.869083936 + 0.00894880345*T - 1.58366345*10^{-5}*T^2 + 7.97543259*10^{-9}*T^3$$ (25)

T in K and Thermal conductivity in W/(m*K)

The density of hybrid nanofluids ρ_{hnf} is calculated from [16]:

$$\rho_{hnf} = \rho_f \left(1-\phi_1\right)\left[\left(1-\phi_2\right)+\phi_2\left(\frac{\rho_2}{\rho_f}\right)\right]+\phi_1\rho_1$$ (26)

The heat capacity of the hybrid nanofluid $(\rho C_p)_{hnf}$ is calculated by [16]:

$$\left(\rho Cp\right)_{hnf} = \left(\rho Cp\right)_f \left(1-\phi_1\right)\left[\left(1-\phi_2\right)+\phi_2\left(\frac{(\rho Cp)_2}{(\rho Cp)_f}\right)\right]+\phi_1\left(\rho Cp\right)_1$$ (27)

The hybrid nanofluid's thermal expansion coefficient is calculated by [16]:

$$\left(\rho\beta\right)_{hnf} = \left(\rho\beta\right)_f \left(1-\phi_1\right)\left[\left(1-\phi_2\right)+\phi_2\left(\frac{(\rho\beta)_2}{(\rho\beta)_f}\right)\right]+\phi_1\left(\rho\beta\right)_1$$ (28)

The thermal conductivity of hybrid nanofluid λ_{hnf} is determined by [16]:

$$\frac{\lambda_{hnf}}{\lambda_{bf}} = \frac{\lambda_1 + (n-1)\lambda_{bf} - (n-1)\phi_1\left(\lambda_{bf}-\lambda_1\right)}{\lambda_1 + (n-1)\lambda_{bf} - \phi_1\left(\lambda_{bf}-\lambda_1\right)}$$ (29)

Where

$$\frac{\lambda_{bf}}{\lambda_f} = \frac{\lambda_2 + (n-1)\lambda_f - (n-1)\phi_2\left(\lambda_f-\lambda_1\right)}{\lambda_2 + (n-1)\lambda_f - \phi_2\left(\lambda_f-\lambda_2\right)}$$ (30)

With n is an empirical form factor. Especially, n equal to six and three for cylindrical and spherical particles, respectively.

The dynamic viscosity of hybrid nanofluid μ_{hnf} given as follows [16]:

$$\mu_{hnf} = \frac{\mu_f}{\left(1-\phi_2\right)^{2.5}\left(1-\phi_1\right)^{2.5}}$$ (31)

7

Given that heat transfer occurs through a hybrid nanofluid in a porous medium, the effective thermal conductivity λ_{eff} in the three phases is as follows:

$$\lambda_{eff} = \left[\lambda_g^n \varepsilon_g + \lambda_{hnf}^n \varepsilon_{hnf} + \lambda_s^n (1 - \varepsilon_s) \right]^{\frac{1}{n}} \tag{32}$$

The thermophysical properties of the porous medium and the hybrid nanofluid [35-37] are constants and provided in Table 1 and 2, respectively.

Tab. 1. Thermophysical properties of used nanoparticles

Physical properties	Al_2O_3	MgO	SiO_2
Density ρ (kg/m^3)	3970	3580	2200
Specific heat Cp (J/kg K)	765	1030	703
Thermal conductivity λ (W/m K)	40	60	1.2

Tab. 2. Physical characteristics of porous media

Physical properties	Values
Porosity ε	0.24
Density ρ_s (Kg.m^{-3})	2600
Specific heat Cp_s (J.Kg^{-1}.K^{-1})	900
Thermal conductivity λ_s (W.m^{-1}.K^{-1})	1.15
Intrinsic permeability K (m^2)	2.5 10^{-4}

3. Resolving and validating numerical code

All the system of equations for both the fluid in the channel and the porous media mentioned with details previously was resolved using the software Comsol Multiphysics based on finite elements method.

After several mesh type tests, the best mesh that corresponds to a good validation of our numerical code with the experimental results is the extra-fine mesh. This type of mesh is shown in figure 2b contains 2430 domain elements and 188 boundary elements.

Our numerical results were compared with the experimental results of Keita's [38]. As a result, we showed in Figure 2, the saturation as a function of time for colloidal particles suspended in a porous medium that are steadily drying. The excellent concordance between our findings and those of Keita [38] can be seen in this graph.
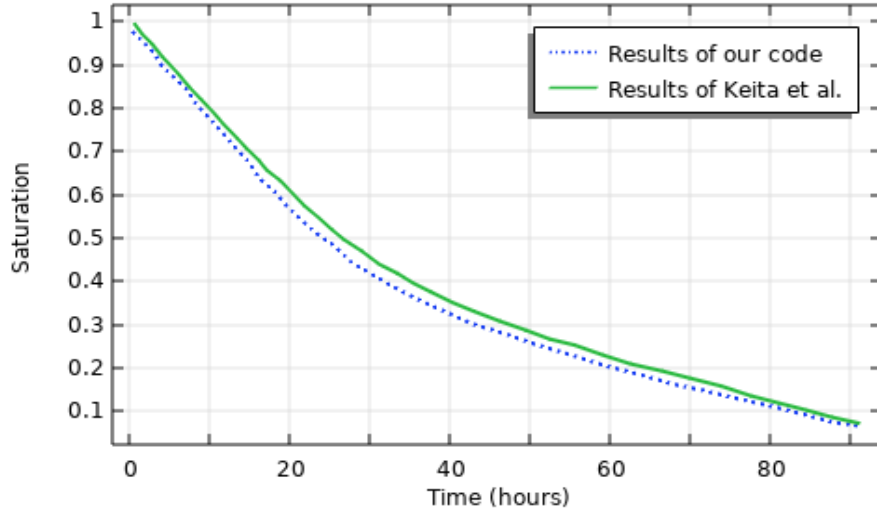
Fig. 2. Time progression of saturation during a porous medium's drying

4. Results and Discussions

4.1. Evolution of the time of several state variables inside the porous media

Figures 3-a and 3-b show the temperature and saturation of hybrid nanofluid as a function of time for the right upper corner node of a porous wall for various numbers of nanoparticle volume fraction φ =0 (clear water) and 0.07. From the figure 3-a, we see that the value of the temperature drops as the volume percentage of nanoparticles rises. The density and viscosity of the hybrid nanofluid appear to rise as the volume percentage of nanoparticles grows. Although effective thermal conductivity rises with nanoparticle volume fraction, viscosity rises at a far faster rate than effective thermal conductivity. As a result, dissipation rises and the flow slows, resulting in reduced transfers.

From the figure 3-b, we see that the hybrid nanofluid saturation for the right upper corner node of the porous wall inside the porous wall decreases with time and will be weak after 10 hours. Because of problems with stability and changes in the fluid's behavior, increasing the concentration of nanoparticles has practical limitations.
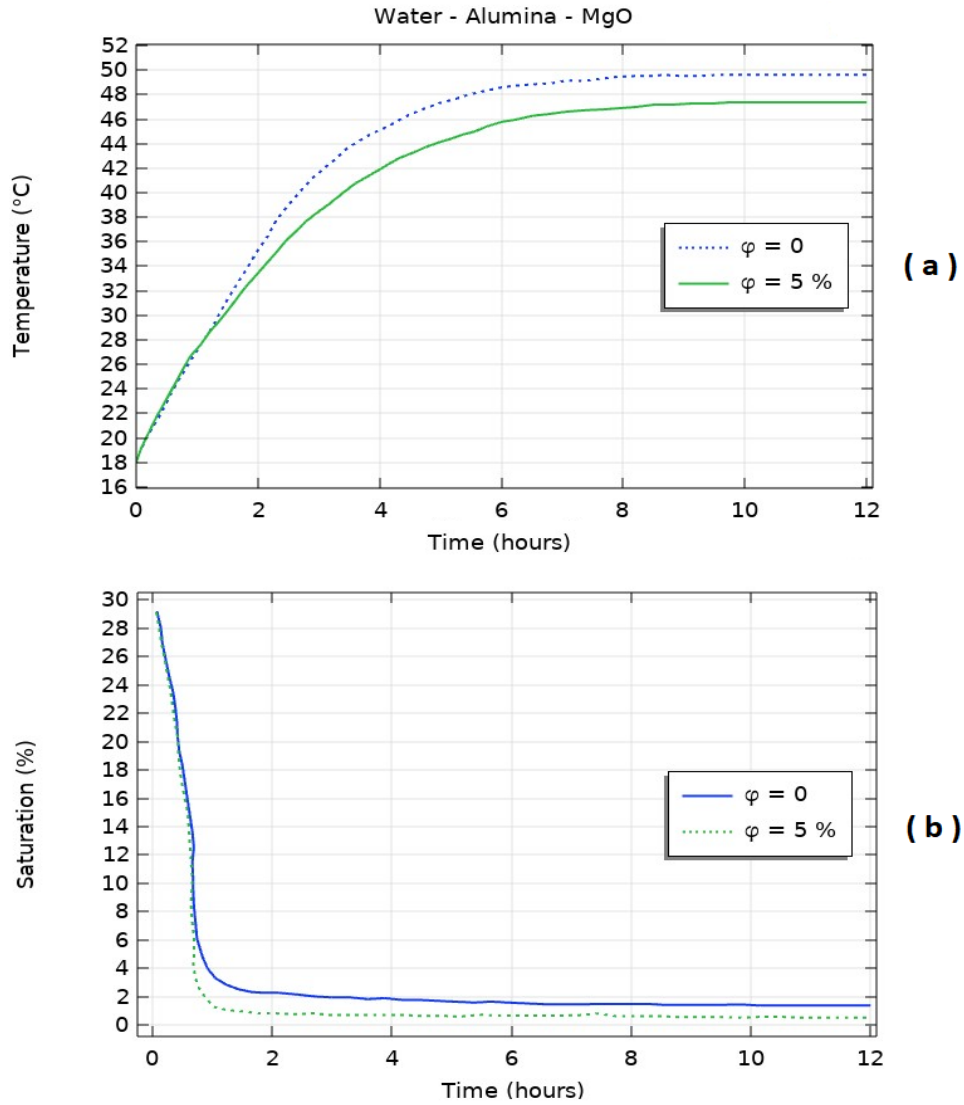
9

Fig. 3. Time progression of the temperature (a) and the saturation of hybrid nanofluid (b) for the right upper corner node of porous wall for 2 various volume fractions of nanoparticles

4.2. Influence of volume fraction of nanoparticle on effective thermal conductivity

Figure 4 depicts the influence of nanoparticle volume fraction on effective thermal conductivity. When the volume fraction of nanoparticles rises from 0 to 5%, the effective thermal conductivity increases. This has the opposite effect and contributes to a 4.4% reduction in the temperature of the porous medium (Fig.3-a).
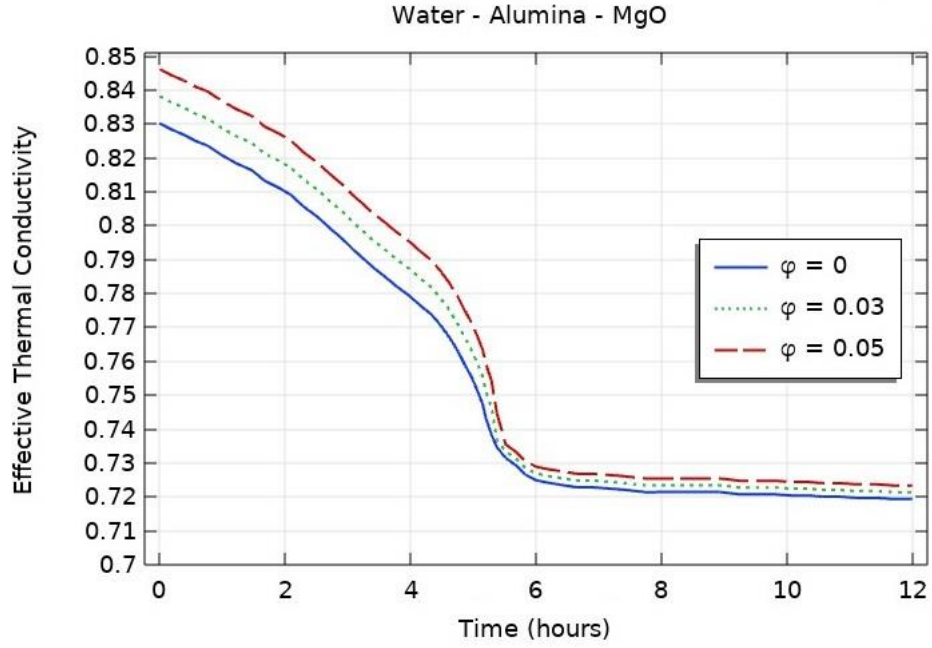
Fig. 4. Time evolution of the effective thermal conductivity for varied nanoparticle volume fractions

4.3. Influence of the ambient temperature

Figures 5-a and 5-b depict the temperature and saturation of hybrid nanofluid in the porous media with time for various ambient temperatures for hybrid nanofluid (Water-Al$_2$O$_3$-MgO) at φ =0.05. From the figure 5-a, we see that the temperature increases with the increase of ambient temperatures. When the temperature reaches 100°C, evaporation begins right away, resulting in rapid drying. The duration of time it takes for the second phase to dry reduces as the ambient temperature rises. From the figure 5-b, we show that the hybrid nanofluid's saturation continuously drops with time until it achieves the minimum saturation.
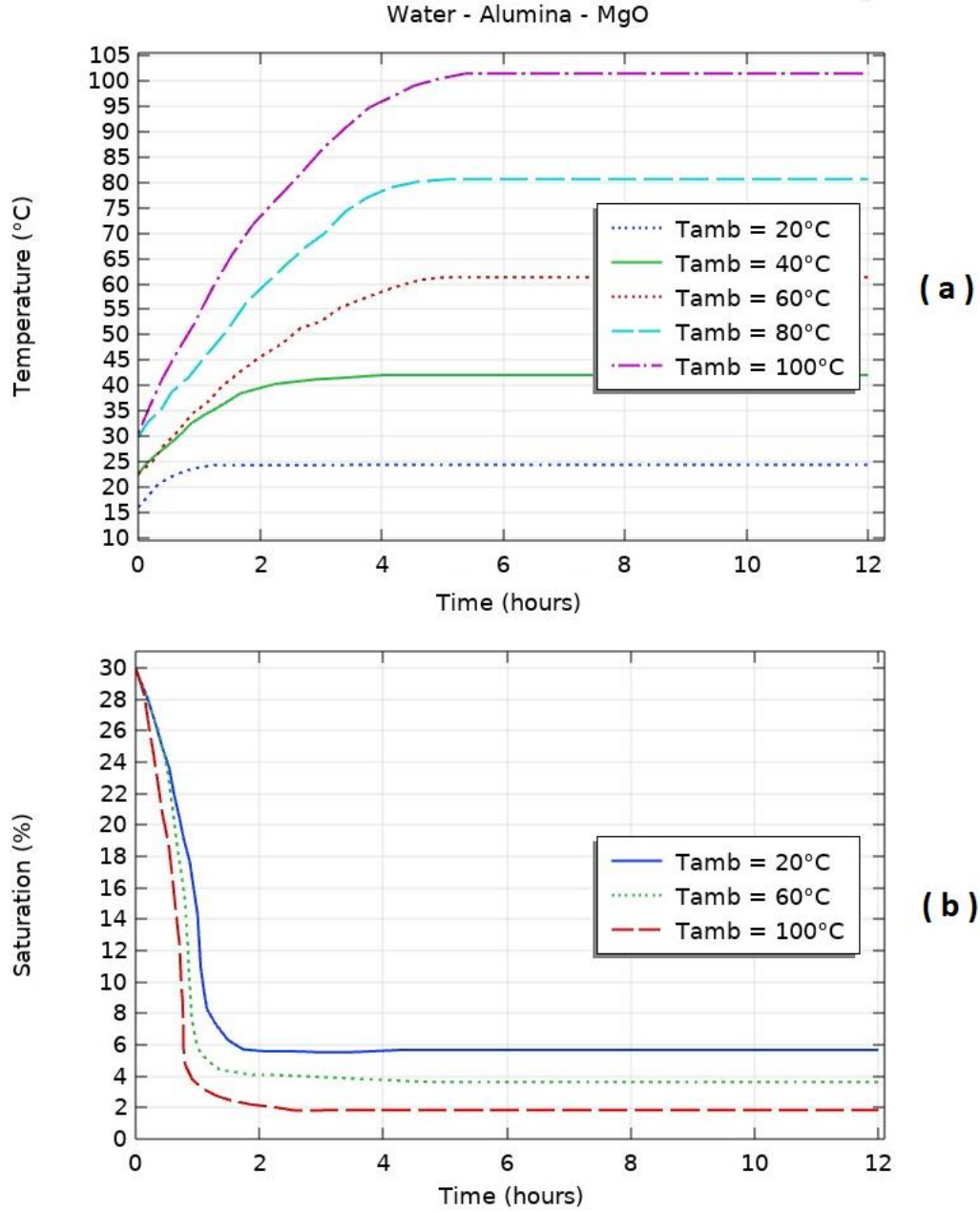
Fig. 5. Influence of ambient temperature on temperature evolution (a) and hybrid nanofluid saturation (b) for the right upper corner node of porous wall

4.4. Influence of the initial hybrid nanofluid saturation

Figures 6a and 6b show the temperature and saturation of a hybrid nanofluid (Water-Al_2O_3-MgO) during time when $\varphi = 0.05$. When the saturation of the hybrid nanofluid drops, the second phase gets shorter and can possibly disappear completely, as shown in Fig. 6-a. This can be explained by the fact that the medium is hygroscopic when it first reaches the drying field. When the initial hybrid nanofluid saturation $S_{ini} = 10\%$, the temperature of the porous medium rises from the start, whereas when $S_{ini} = 40\%$, it follows the traditional profile that can be seen during the different phases.
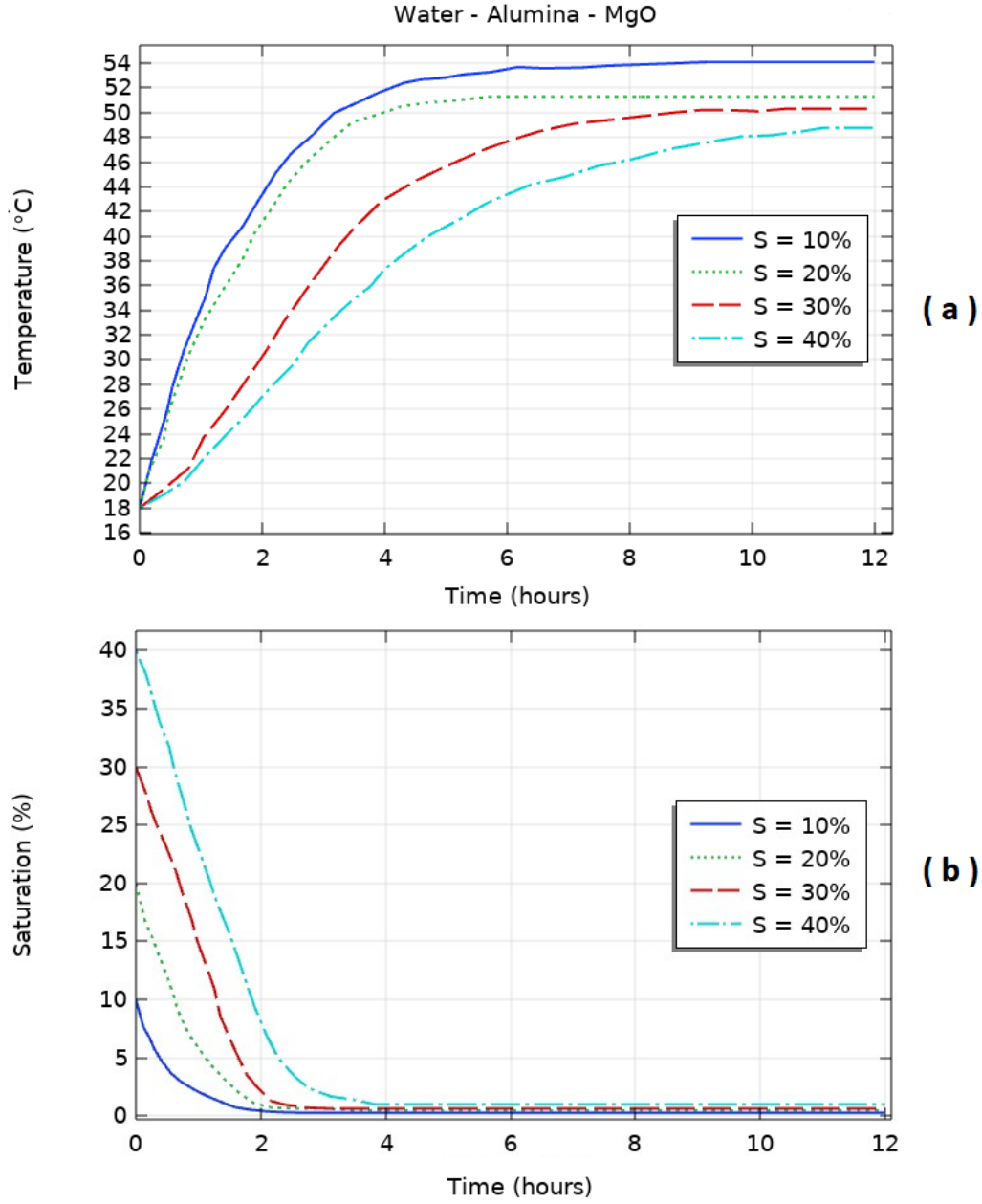
Fig. 6. Influence of initial hybrid nanofluid saturation on temperature evolution (a) and hybrid nanofluid saturation (b) for the right upper corner node of porous wall

4.5. Influence of natural convection on the evolution of various state variables

(Fig. 7-a) and (Fig. 7-b) shows respectively, the local heat and mass transfer coefficients htx, hmx for hybrid nanofluid (Water-Al$_2$O$_3$-MgO) when $\varphi = 0.05$ for the center node of porous wall.

From these figures, we observe that the natural convection has a considerable impact on the drying processes. This is mostly owing to the substantial differences seen between the interface and ambient temperatures and between the interface and ambient vapor concentrations on the one hand.
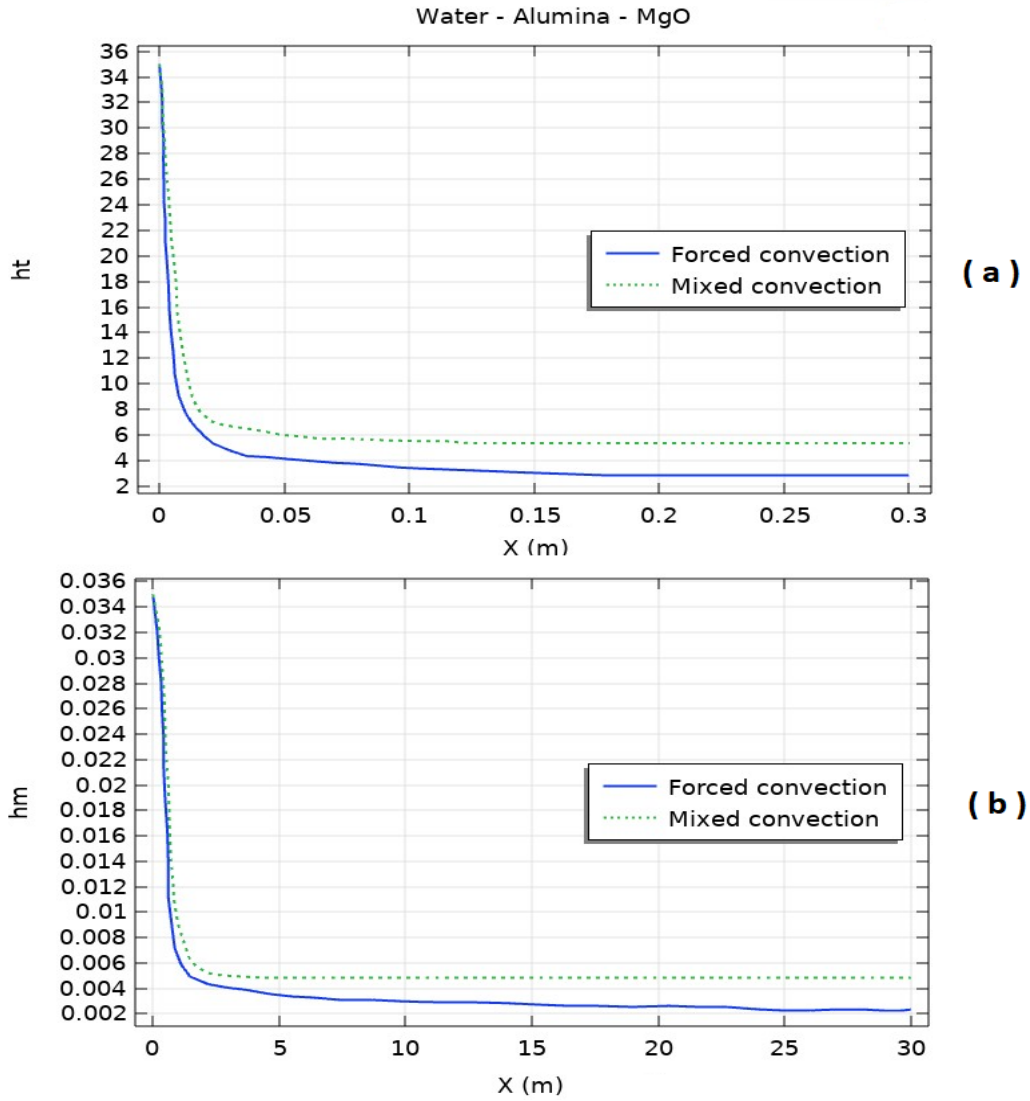
Fig. 7. Evolution of local mass and heat transfer coefficients ((a) htx, (b) hmx)

4.6. Influence of the type of nanoparticle

For a better comparison between different types of nanohybrids, we choose nanoparticles that can really be used in the case of bricks, which are MgO (magnesium oxide) and SiO_2 (silica) and at the same time have the highest thermophysical properties for our industrial application.

Figure 8 indicates the temperature of hybrid nanofluid as a function of time for these two different types of nanoparticles when $\varphi = 0.05$ for the right upper corner node of a porous wall. As compared to hybrid nanofluid (Water-Al_2O_3-MgO), it can be noticed that the transfers are higher in (Water-Al_2O_3-MgO) than in (Water-Al_2O_3-SiO_2) because (Water-Al_2O_3-MgO) has a lower density, viscosity, and thermal conductivity than (Water-Al_2O_3-SiO_2), which generally promotes an increase in transfers (Water-Al_2O_3-MgO). Using the nanohybrid (Water-Al_2O_3-SiO_2), the temperature is reduced by 4%.
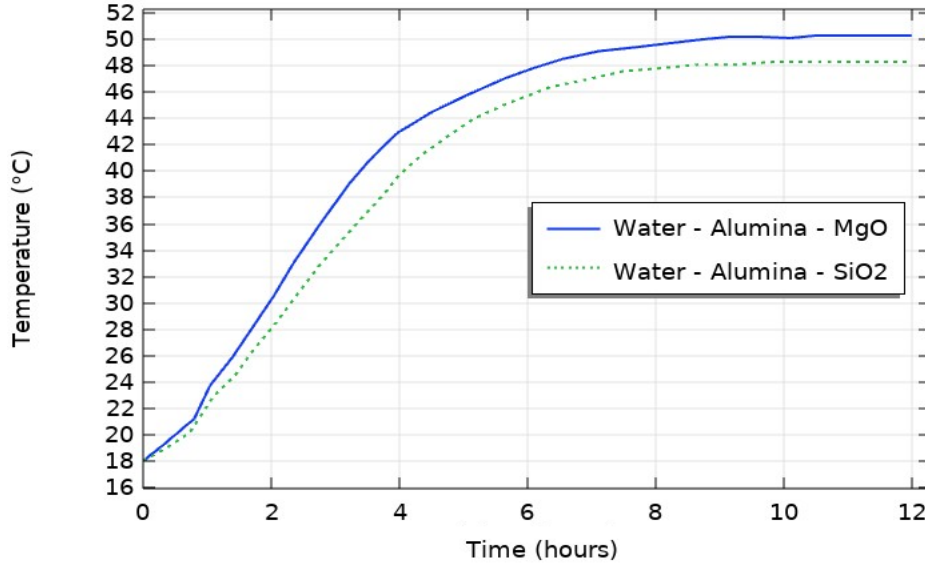
14

Fig. 8. Temperature variation during time for the porous wall's right upper corner node and two types of nanoparticles

5. Conclusion

The current research focuses on a numerical simulation of two-dimensional mass and heat transfer during mixed convective drying of an unsaturated porous wall with hybrid nanofluid. The numerical resolution was done using the software Comsol Multiphysics. After validation of our model, the influence of the nanoparticle volume fraction, ambient temperature, initial hybrid nanofluid saturation, and nanoparticle type on heat and mass transport was investigated. The results reveal that introducing nanoparticles has a significant effect and that as the volume fraction of nanoparticles increases, the temperature of the porous medium decreases considerably. Compared to Water-Al_2O_3-SiO_2, Water-Al_2O_3-MgO has a higher heat and mass transfer, and the temperature is reduced by 4%. As the ambient temperature rises, the time it takes for the second phase to dry decreases.

Nomenclature

C_{ps} - Specific heat of porous medium (J.kg^{-1}.K^{-1})

D_v - Vapor diffusion coefficient into air (m^2.s^{-1})

e - Thickness of porous wall (m)

e - Thickness of porous wall (m

G - Gravitational constant (m.s^{-2})

Gr_m - Mass transfer Grashof number, $\left(=g\beta(C_v-C_{v0})E^3/v^2\right)$

h_{mx} - Local mass transfer coefficient (m.s^{-1})

h_t - Average heat transfer coefficient (W.m^{-2}.K^{-1})

h_{tx} - Local heat transfer coefficient (W.m^{-2}.K^{-1})

K - Permeability of porous medium (m^2)

M - Molecular weight (Kg)

$\dot{m}_v$ - Mass rate of evaporation (Kg.m^{-2}.s^{-1})

P_c - Capillary pressure (Pa)

R - Universal gas constant (J.$mole^{-1}$.K^{-1})

r - Curve ray (m)

S - Saturation (%)

T - Temperature (K)

t - Time (s)

U - Longitudinal velocity (m.s^{-1})

V - Transverse velocity (m.s^{-1})

W - Channel width (m)

x - Longitudinal direction (m)

y - Transverse direction (m)

15

Subscripts

a - Dry air

eff - Effective

f - Base fluid

g - Gas (air-water vapor mixture)

hnf - Hybrid nanofluid

ini - Initial

int - Interface

l - Liquid

np - Nanoparticle

o - Ambient

r - Right face

l - Liquid

s - Solid

v - Water vapor

vs - Saturated vapor

x - Local

Greek symbols

β - Coefficient of thermal expansion (K^{-1})

ρ - Density (Kg.m^{-3})

σ - Superficial tension (N.m^{-1})

ρ_{hnf} - Density of the hybrid nanofluid (Kg.m^{-3})

$(\rho C_p)_{hnf}$ - Heat capacity of the hybrid nanofluid

λ - Thermal conductivity (W.m^{-1}.K^{-1})

λ_{hnf} - Thermal conductivity of the hybrid nanofluid (W.m^{-1}.K^{-1})

μ_{hnf} - Dynamic viscosity of the hybrid nanofluid (Kg.m^{-1}.s^{-1})

ΔH_{vap} - Latent heat of vaporization (J.Kg^{-1})

References

[1] Hacihafizoglu, O., *et al.*, Numerical Investigation of Intermittent Drying of a Corn for Different Drying Conditions, *Thermal Science*, 23 (2019), 2A, pp. 801-812.

[2] Kanevce, L. *et al.*, Application of Inverse Concepts to Drying, *Thermal Science*, 9 (2005), 2, pp. 31-44.

[3] Massoudi, M.D., et al., MHD Heat Transfer in W-Shaped Inclined Cavity Containing a Porous Medium Saturated with Ag/Al$_2$O$_3$ Hybrid Nanofluid in the Presence of Uniform Heat Generation/Absorption, *Energies*, 13 (2020), 13, pp. 3457.

[4] Zidan, A. M., et al., Entropy-based analysis and economic scrutiny of magneto thermal natural convection enhancement in a nanofluid-filled porous trapezium-shaped cavity having localized baffles. *Waves in Random and Complex Media*, (2022), p. 1-21.

[5] Massoudi, M.D., et al., Free convection and thermal radiation of nanofluid inside nonagon inclined cavity containing a porous medium influenced by magnetic field with variable direction in the presence of uniform heat generation/absorption, *International Journal of Numerical Methods for Heat and Fluid Flow*, 31, (2020), 3, pp. 933-958.

[6] Massoudi, M.D., *et al.,* Numerical analysis of magneto-natural convection and thermal radiation of SWCNT nanofluid inside T-inverted shaped corrugated cavity containing porous medium, *International journal of numerical methods for heat and fluid flow*, 32 (2021), 3, pp. 1092-1114.

[7] Kadem, S., *et al.,* Transient Analysis of Heat and Mass Transfer During Heat Treatment of Wood Including Pressure Equation, *Thermal Science, 19* (2015), 2, pp. 693-702.

[8] Zidan, A.M. *et al.,* Thermal management and natural convection flow of nano encapsulated phase change material (NEPCM)-water suspension in a reverse T-shaped porous cavity enshrining two hot corrugated baffles: A boost to renewable energy storage, *Journal of Building Engineering*, 53, (2022), pp.104550.

[9] Pamuk, M.T., Numerical Study of Heat Transfer in a Porous Medium of Steel Balls, *Thermal Science, 23* (2019), 1, pp. 271-279.

[10] Ben Hamida, M.B., et *al.*, Numerical study of heat and mass transfer enhancement for bubble absorption process of ammonia-water mixture without and with nanofluids, *Thermal Science*, 22 (2018), (6 Part B), pp. 3107-3120.

[11] Massoudi, M.D, Ben Hamida, M.B., Free convection and thermal radiation of a nanofluid inside an inclined L-shaped microelectronic module under the Lorentz forces' impact, *Heat transfer-asian research,* 50 (2021), 3, pp. 2849-2873.

[12] Ben Hamida, M.B. Hatami, M., Optimization of fins arrangements for the square light emitting diode (LED) cooling through nanofluid-filled microchannel, *Scientific Reports*, 11 (2021), 1, pp. 12610.

[13] Izadi, M., et *al.*, Numerical study on forced convection heat transfer of TiO_2/water nanofluid flow inside a double-pipe heat exchanger with spindle-shaped turbulators, *Engineering Analysis with Boundary Elements,* 150 (2023), pp. 612-623.

[14] Ben Hamida, M.B., et *al.*, Heat and mass transfer enhancement for falling film absorption process in vertical plate absorber by adding Copper nanoparticles, *Arabian Journal for Science and Engineering*, 43 (2018), pp. 4991-5001.

[15] Massoudi, M.D., *et al.,* Numerical evaluation of MHD SWCNT-water nanoliquid performance in cooling an electronic heat sink featuring twisted hexagonal fins considering thermal emission impact: Comparison between various fins shapes, *Sustainable Energy Technologies and Assessments*, 53 (2022), Part A, pp. 102350.

[16] Ben Hamida, M.B., et *al.*, Natural Convection Heat Transfer in an Enclosure Filled with an Ethylene Glycol-Copper Nanofluid Under Magnetic Fields, *Numerical Heat Transfer, Part A: Applications: An International Journal of Computation and Methodology*, 67 (2014), 8, pp. 902–920.

[17] Massoudi, M.D., *et al.,* Effects of L-shaped fins on cooling an electronic heat sink fitted under magnetic field of CNT–water/ethylene glycol nanoliquid, *European Physical Journal Plus*, 137 (2022), 7, pp. 843.

[18] Alzahrani, A. K., *et al*., The unsteady liquid film flow of the carbon nanotubes engine oil nanofluid over a non-linear radially extending surface, *Thermal Science*, 24 (2020), 2A, pp. 951-963.

[19] Sheikholeslami, M., Modeling investigation for energy storage system including mixture of paraffin and ZnO nano-powders considering porous media, *Journal of Petroleum Science and Engineering*, 219, (2022), pp. 111066.

[20] Ben Hamida, M.B., *et al*., Potential of Tubular Solar Still with Rectangular Trough for Water Production under Vacuum Condition, *Thermal Science*, 26, (2022), 5B, pp. 4271-4283.

[21] Massoudi, M.D., Ben Hamida, M.B., MHD natural convection and thermal radiation of diamond–water nanofluid around rotating elliptical baffle inside inclined trapezoidal cavity, *The European Physical Journal Plus*, 135 (2020), 902, pp.1-24.

[22] Alshammari, F., et al., Effects of Working Fluid Type on Powertrain Performance and Turbine Design Using Experimental Data of a 7.25ℓ Heavy-Duty Diesel Engine, *Energy conversion and Management*, 231, (2021), pp. 113828.

[23] Massoudi, M.D., *et al.,* The influence of multiple fins arrangement cases on heat sink efficiency of MHD MWCNT-water nanofluid within tilted T-shaped cavity packed with trapezoidal fins considering thermal emission impact, *International Communications in Heat and Mass Transfer*, 126 (2021), pp. 105468.

[24] Massoudi, M. D., Ben Hamida, M. B., Enhancement of MHD radiative CNT-50% water + 50% ethylene glycol nanoliquid performance in cooling an electronic heat sink featuring wavy fins, *Waves in Random and Complex Media*, (2022), pp. 1-26.

[25] Sheikholeslami, M., Jafaryar, M., Thermal assessment of solar concentrated system with utilizing CNT nanoparticles and complicated helical turbulator, *International Journal of Thermal Sciences*, 184, (2023), pp. 108015.

[26] Sheikholeslami, M., Ebrahimpour, Z., Thermal improvement of linear Fresnel solar system utilizing Al_2O_3-water nanofluid and multi-way twisted tape, *International Journal of Thermal Sciences*, 176, (2022), 107505.

[27] Ben Jaballah, R., et *al.*, Enhancement of the performance of bubble absorber using hybrid nanofluid as a cooled absorption system, *International journal of numerical methods for heat and fluid flow*, 29 (2019), 10, pp. 3857-3871.

[28] Ben Jaballah, R., et *al.*, The influence of hybrid nanofluid and coolant Flow direction on bubble mode absorption improvement, *Mathematical Methods in the Applied Sciences*, (2020), pp. 1-15, DOI:10.1002/mma.6605

[29] Ben Hamida, M.B., Hatami, M., Optimization of fins arrangements for the square light emitting diode (LED) cooling through nanofluid-filled microchannel, *Scientific Reports*, 11 (2021), 1, pp. 12610.

[30] Abbasi, FM., et *al.*, Thermodynamic analysis of electroosmosis regulated peristaltic motion of Fe_3O_4–Cu/H_2O hybrid nanofluid, *International Journal of Modern Physics B*, 36 (2022), 14, 2250060.

[31] Sheikholeslami, M., Numerical investigation of solar system equipped with innovative turbulator and hybrid nanofluid, *Solar Energy Materials and Solar Cells*, 243 (2022), pp. 111786.

[32] Ben Hamida, M.B., Hatami, M., Investigation of heated fins geometries on the heat transfer of a channel filled by hybrid nanofluids under the electric field, *Case Studies in Thermal Engineering*, 28 (2021), 101450.

[33] Mobarki, A., *et al.,* The Variability Effect of Fluid Thermophysical Properties on Convective Drying of Unsaturated Porous Media, *Int Journal of Heat and Technology, 21* (2003), 2, pp. 89-97.

[34] Ben Hamida, M.B., et *al.*, A three-dimensional thermal analysis for cooling a square Light Emitting Diode by Multiwalled Carbon Nanotube-nanofluid-filled in a rectangular microchannel, *Advances in Mechanical Engineering*, 13 (2021), 11, pp.1–14.

[35] Hussein, A. K., et *al.*, Magneto-hydrodynamic natural convection in an inclined T-shaped enclosure for different nanofluids and subjected to a uniform heat source, *Alexandria Engineering Journal*, 55, (2016), 3, pp. 2157-2169.

[36] Ben Hamida, M.B., Numerical analysis of tubular solar still with rectangular and cylindrical troughs for water production under vacuum, *Journal of Taibah University for Science*, 17, (2023), 1, pp. 2159172.

[37] Yıldız C., *et al.*, Comparison of a theoretical and experimental thermal conductivity model on the heat transfer performance of Al_2O_3-SiO_2/water hybrid-nanofluid, *International Journal of Heat and Mass Transfer*, 140, (2019), 598-605.

[38] Keita, E., *et al.*, MRI Evidence for a Receding-Front Effect in Drying Porous Media, *Physical Review E*, 87 (2013), pp. 1-6.